

Supporting Information

Confined Catalysts Inside CNTs Derived from 2D Metal-Organic Framework for Electrolysis

Qinghua Xia,^{b,‡} Haimin Liu,^{a,‡} Mengmeng Jin,^a Linfei Lai,^{a,c*} Yongting Qiu,^a Haili Zhai,^a
Hongbo Li,^{b*} Xiang Liu^{d*}

a. Key Laboratory of Flexible Electronics & Institute of Advanced Materials (IAM), Jiangsu National Synergistic Innovation Center for Advanced Materials (SICAM), Nanjing Tech University, 5 XinMofan Road, Nanjing 210009

b. Yanshan branch of Beijing Research Institute of Chemical Industry, Sinopec, Beijing 102500, China. E-mail: lihongbo.bjhy@sinopec.com

c. CINTRA CNRS/NTU/Thales, UMI 3288, 50 Nanyang Drive, 637553, Singapore. E-mail: linfei.lai@ntu.edu.sg

d. School of Energy Science and Engineering, Nanjing Tech University, 30 South Puzhu Road, Nanjing 211816, China. E-mail: iamxliu@njtech.edu.cn

1. Experimental Section

1.1 Materials

All chemical reagents were purchased and used without any further purification from commercial sources: cobalt nitrate hexahydrate (99%, Aladdin), p-phthalic acid (99%, Sinopharm Chemical Reagent Co. Ltd.), N, N-dimethylformamide (DMF, Sinopharm Chemical Reagent Co. Ltd.), and ethanol (C₂H₅OH, Wuxi Yasheng Chemical Reagent Co. Ltd.). All aqueous solution has been prepared with high-purity de-ionized water (DI-water, resistance 18 MΩ cm⁻¹).

1.2 Synthesis of Co-MOF/H₂ and Co-MOF/Ar

In a typical procedure, 2D Co-MOF nanosheets were synthesized by a surfactant-assisted solvothermal route. Typically, a solution of cobalt nitrate hexahydrate (0.859 mmol, 250 mg) in 20 mL deionized water was added to a solution of 1,4-benzenedicarboxylate (0.4295 mmol, 71.4 mg) in 40 mL DMF/C₂H₅OH (1:1 v/v) and mixed to obtain a stable solution, and then 250 mg polyvinylpyrrolidone (PVP) was added to the solution with stirring. The resulting solution was then transferred into a 100 mL Teflon-lined stainless steel autoclave with a piece of cleaned nickel foam (2×3 cm²) immersed into the aqueous solution. After sealing, the autoclave was heated at 80 °C for 60 h, and then naturally cooled to room temperature. Afterwards, the obtained samples were washed using deionized water and ethanol to remove impurities and dried in the air naturally. Finally, the NF-CoMOF was heated at 600 °C for 2 h at a ramp rate of 2 °C min⁻¹ under H₂ and Ar, respectively.

1.3 Material Characterization

Scanning electron microscopy (SEM) was conducted on JEOL JSM-7800 at an accelerating voltage of 3 kV. Transmission electron microscopy (TEM) was carried out on a JEOL-2100 transmission electron microscope at an acceleration voltage of 120 kV. X-ray diffraction patterns were recorded on a Smart lab with Cu K α radiation. X-ray photoelectron spectroscopy (XPS) analysis was measured by Thermo ESCALAB 250XI with Al K α (1846.6 eV) X-ray source.

1.4 The geometrical phase analysis (GPA)

The GPA combines real-space and Fourier-space information of an atomic resolution HRTEM or HAADF-STEM image to measure displacements.[1] The periodic phase in the image **needs** to be obtained, by calculating the local Fourier components, which are determined through Fourier filtering:[2]

$$I_g = A_g e^{iP_g} \quad (1)$$

where A_g and P_g are the amplitude and the phase of the Fourier component, respectively.

The phase can be related to the displacement field by the following equation:

$$P_g = -2\pi \mathbf{g} \cdot \mathbf{u} \quad (2)$$

where \mathbf{g} is the reciprocal lattice vector and \mathbf{u} is the displacement field. Two-phase images whose reciprocal lattice vectors are not parallel are needed. Then the displacement field can be determined by these phase images.[3, 4]

Given the geometric phase of two Fourier components, the displacement field can be determined:[2]

$$\mathbf{u}(\mathbf{r}) = \frac{1}{-2\pi} [P_{\mathbf{g}_1}(\mathbf{r})\mathbf{a}_1 + P_{\mathbf{g}_2}(\mathbf{r})\mathbf{a}_2] \quad (2)$$

where \mathbf{a}_1 and \mathbf{a}_2 are the real-space basis vectors corresponding to the reciprocal lattice defined by \mathbf{g}_1 and \mathbf{g}_2 (i.e. $\mathbf{a}_i \cdot \mathbf{g}_j = \delta_{ij}$). Then, the derivation of the displacement field gives the strain field in two principal directions:[5]

$$\varepsilon_{xx} = \partial u_x(\mathbf{r}) / \partial x, \varepsilon_{yy} = \partial u_y(\mathbf{r}) / \partial y, \varepsilon_{xy} = \frac{1}{2} [\partial u_x(\mathbf{r}) / \partial x + \partial u_y(\mathbf{r}) / \partial y]$$

1.5 Electrochemical measurements

HER and OER performance of the above-prepared samples were conducted on the CHI660E with a standard three-electrode system in 1 M KOH. The electrolyte was purged with nitrogen before the tests. A graphite rod and an Ag/AgCl electrode (3.5 M KCl) were utilized as the counter electrode and the reference electrode, respectively. **The free-standing electrode was directly applied as the working electrode.** LSV curves of the prepared samples were measured at a scan rate of 5 mV s⁻¹. All the potentials measured were calibrated to RHE (without *iR*-compensation), according to the equation of E(RHE) = E(Ag/AgCl) + 0.205 + 0.059 × pH. **The potential range of HER measurement is -0.6~ 0.1 V vs RHE. Besides, OER measurement was assessed at the potential range of 1.2 ~2.0 V vs RHE. Before the LSV test, the cyclic voltammogram (CV) plot in the non-faradaic region was performed to activate the catalyst.** EIS measurements were performed in potentiostatic mode at a frequency range of 0.1 Hz to 100 kHz. The double-layer capacitance (C_{dl}) calculated from cyclic voltammogram curves has been used to determine the ESCA of the as-prepared sample. CV plots were obtained in non-Faradaic region (0.15-0.25 V vs RHE) at the eight different scan rates (125, 100, 85, 70, 55, 40, 25 and 10 mV s⁻¹). Chronopotentiometric measurements were harnessed

to study the long-term durability (without iR compensated). The catalytic performance towards overall water splitting was typically investigated in a two-electrode system. Co-MOF/H₂ electrodes were directly used as both cathode and anode.

2. Figures and graphs

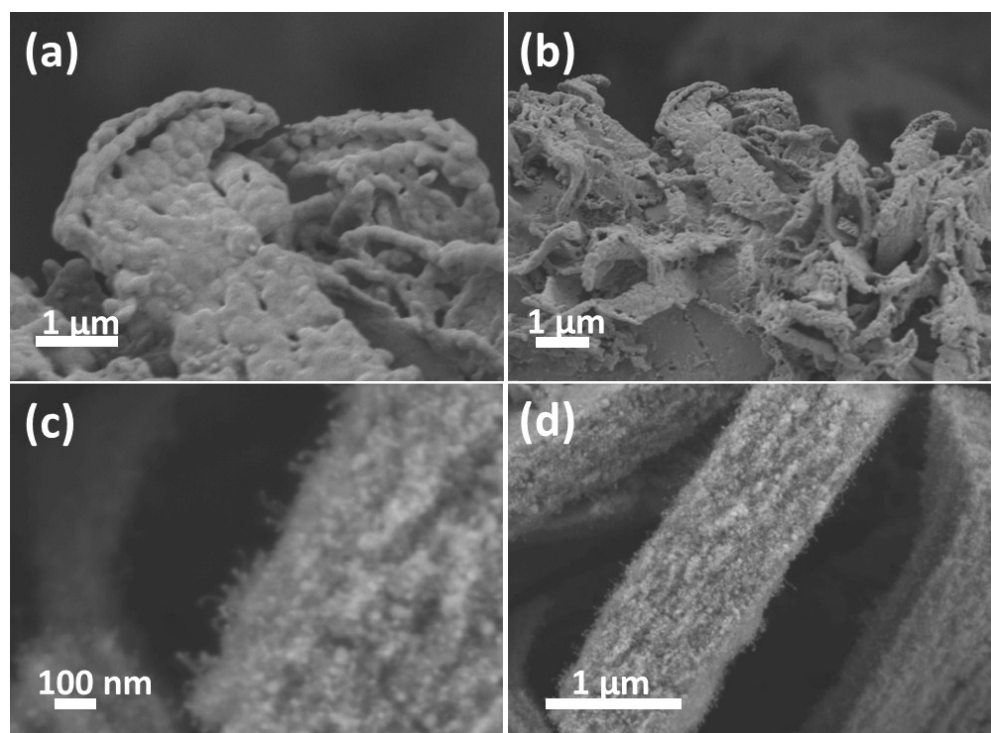


Figure S1. The SEM images of a,b) Co-MOF/Ar, c,d) Co-MOF/H₂.

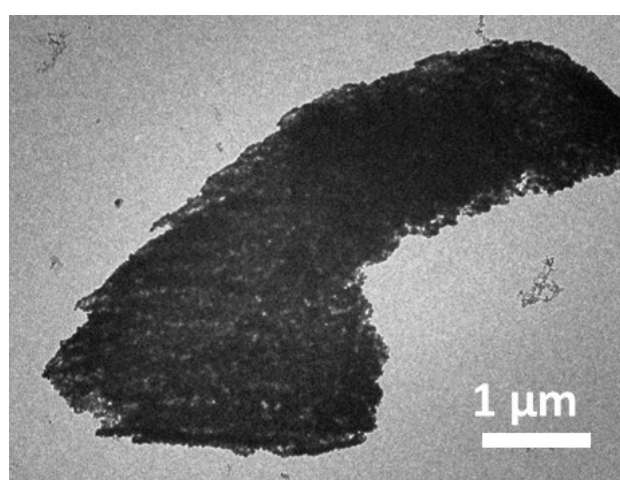


Figure S2. The TEM image of Co-MOF/Ar.

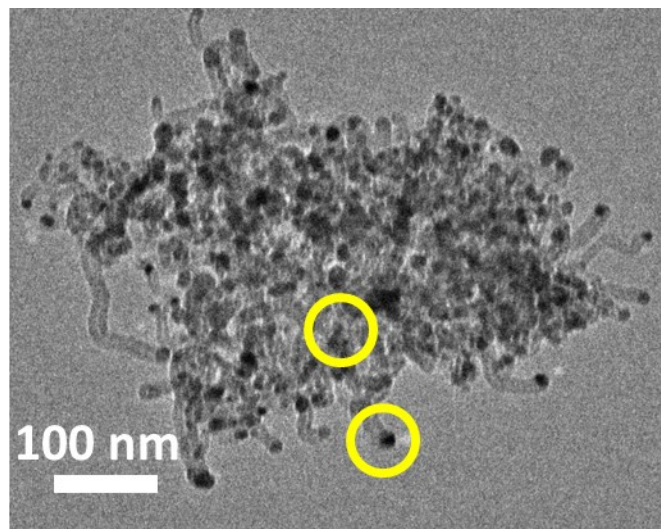


Figure S3. The TEM image of Co-MOF/H₂.

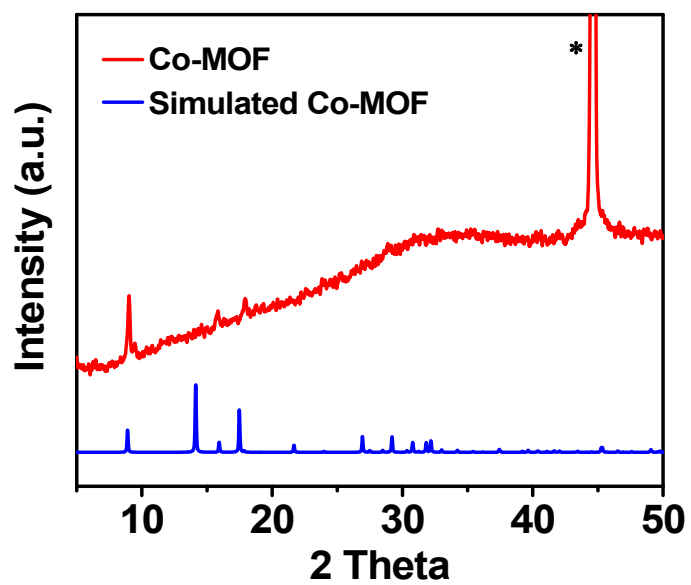


Figure S4. XRD pattern of Co-MOF grown in NF.

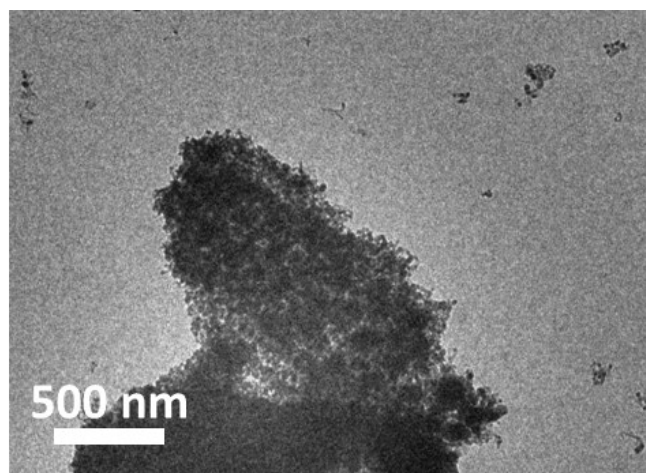


Figure S5. The TEM image of Co-MOF/H₂ subjected to HER durability test.

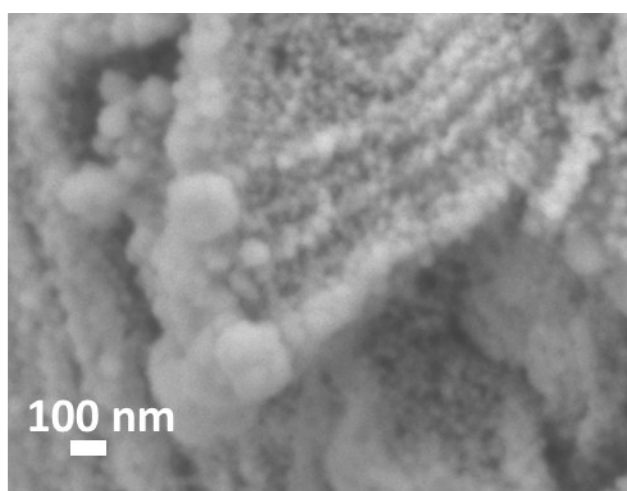


Figure S6. The SEM image of Co-MOF/H₂ subjected to OER durability test.

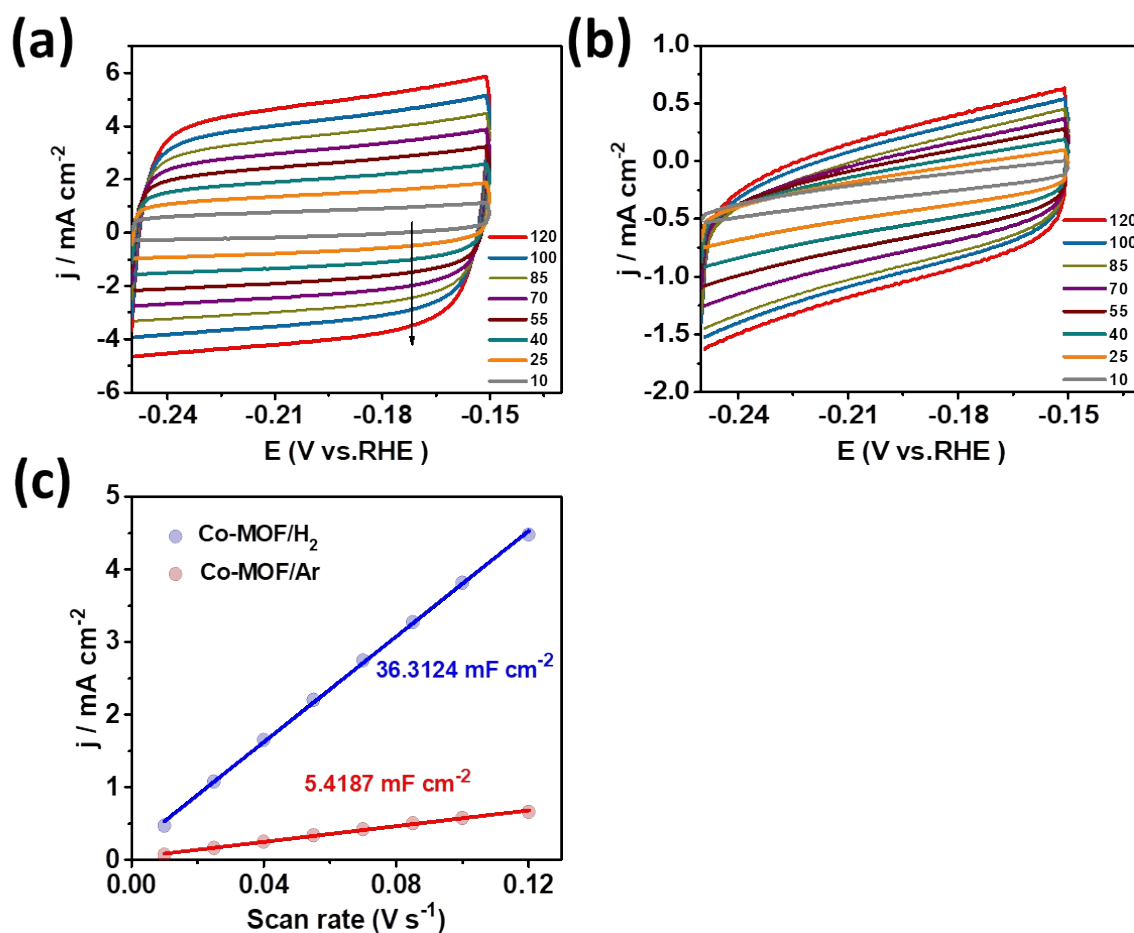
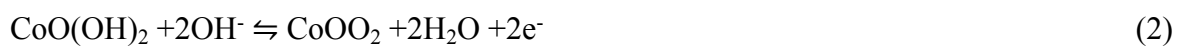


Figure S7. Cyclic voltammogram recorded at different scan rates in the region of 0.15-0.25 V vs RHE for the determination of the double-layer capacitance (C_{dl}), a) Co-MOF/ H_2 , b) Co-MOF/Ar. c) C_{dl} values of Co-MOF/ H_2 and Co-MOF/Ar.

Materials	Substrates	Electrolytes	$\eta@10 \text{ mA cm}^{-2}$ (V)	References
Co-MOF/H ₂	Nickel foam	1 M KOH	1.619	This work
Ni ₃ S ₂ /NF	Nickel foam	1 M KOH	1.68	[6]
MoP/NF	Nickel foam	1 M KOH	1.62	[7]
NFN-MOF/NF	Nickel foam	1 M KOH	1.56	[8]
Co-Ni-Se/C/NF	Nickel foam	1 M KOH	1.60	[9]
Mo-W-S-2@Ni ₃ S ₂	Nickel foam	1 M KOH	1.62	[10]
CoS _x /Ni ₃ S ₂	Nickel foam	1 M KOH	1.57	[11]
Co(OH) ₂ @NCNTs@NF	Nickel foam	1 M KOH	1.72	[12]
NiS/Ni ₂ P/CC	Carbon cloth	1 M KOH	1.67	[13]

Table S1. Comparison of overall water splitting activities of various catalysts.

The mechanism of OER process:



The HER mechanism:



References

- [1] A. Pofelski, S.Y. Woo, B.H. Le, X. Liu, S. Zhao, Z. Mi, S. Löffler, G.A. Botton, 2D strain mapping using scanning transmission electron microscopy Moiré interferometry and geometrical phase analysis, *Ultramicroscopy*, 187 (2018) 1-12.
- [2] M.J. Hÿtch, E. Snoeck, R. Kilaas, Quantitative measurement of displacement and strain fields from HREM micrographs, *Ultramicroscopy*, 74 (1998) 131-146.
- [3] Y. Xiong, H. Shan, Z. Zhou, Y. Yan, W. Chen, Y. Yang, Y. Liu, H. Tian, J. Wu, H. Zhang, D. Yang, Tuning Surface Structure and Strain in Pd-Pt Core-Shell Nanocrystals for Enhanced Electrocatalytic Oxygen Reduction, *Small*, 13 (2017).
- [4] J. Chung, L. Rabenberg, Effects of strain gradients on strain measurements using geometrical phase analysis in the transmission electron microscope, *Ultramicroscopy*, 108 (2008) 1595-1602.
- [5] Y. Wang, J. Yu, X. Zhang, A geometric phase analysis method dedicated to nanomaterials orienting along high-index zone axis, *Micron*, 113 (2018) 20-23.
- [6] G. Ren, Q. Hao, J. Mao, L. Liang, H. Liu, C. Liu, J. Zhang, Ultrafast fabrication of nickel sulfide film on Ni foam for efficient overall water splitting, *Nanoscale*, 10 (2018) 17347-17353.
- [7] Y. Jiang, Y. Lu, J. Lin, X. Wang, Z. Shen, A Hierarchical MoP Nanoflake Array Supported on Ni Foam: A Bifunctional Electrocatalyst for Overall Water Splitting, *Small Methods*, 2 (2018) 1700369.
- [8] D. Senthil Raja, X.-F. Chuah, S.-Y. Lu, In Situ Grown Bimetallic MOF-Based Composite as Highly Efficient Bifunctional Electrocatalyst for Overall Water Splitting with Ultrastability at High Current Densities, *Adv. Energy Mater.*, 8 (2018) 1801065.
- [9] F. Ming, H. Liang, H. Shi, X. Xu, G. Mei, Z. Wang, MOF-derived Co-doped nickel selenide/C electrocatalysts supported on Ni foam for overall water splitting, *J. Mater. Chem. A*, 4 (2016) 15148-15155.
- [10] M. Zheng, J. Du, B. Hou, C.-L. Xu, Few-Layered Mo(1-x)WxS2 Hollow Nanospheres on Ni3S2 Nanorod Heterostructure as Robust Electrocatalysts for Overall Water Splitting, *ACS Appl. Mater. Interfaces*, 9 (2017) 26066-26076.
- [11] S. Shit, S. Chhetri, W. Jang, N.C. Murmu, H. Koo, P. Samanta, T. Kuila, Cobalt Sulfide/Nickel Sulfide

Heterostructure Directly Grown on Nickel Foam: An Efficient and Durable Electrocatalyst for Overall Water Splitting Application, ACS Appl. Mater. Interfaces, 10 (2018) 27712-27722.

[12] P. Guo, J. Wu, X.-B. Li, J. Luo, W.-M. Lau, H. Liu, X.-L. Sun, L.-M. Liu, A highly stable bifunctional catalyst based on 3D Co(OH)₂@NCNTs@NF towards overall water-splitting, Nano Energy, 47 (2018) 96-104.

[13] X. Xiao, D. Huang, Y. Fu, M. Wen, X. Jiang, X. Lv, M. Li, L. Gao, S. Liu, M. Wang, C. Zhao, Y. Shen, Engineering NiS/Ni₂P Heterostructures for Efficient Electrocatalytic Water Splitting, ACS Appl. Mater. Interfaces, 10 (2018) 4689-4696.